Journal of Electronic Imaging 9(4), 432–444 (October 2000).

# Colorimetric modeling for vision systems

**Gao-Wei Chang**
**Yung-Chang Chen***
National Tsing Hua University
Department of Electrical Engineering
Hsinchu, Taiwan 30043, Republic of China

**Abstract.** *A colorimetric modeling technique is proposed to give a computational model associated with colorimetry so that the representation of color acquired from camera imaging is accurate and meaningful. First of all, the camera spectral responses are estimated and the colorimetric quality is evaluated to reveal the feasibility of this work. In the modeling process, we present a spectral matching method and an approach of determining a reference-white luminance. As a result, the acquired color and the true (or measured) color can be well coordinated, with the strength of a global illumination or display white, in a perceptually uniform color space, e.g., in CIE 1976 L*a*b* space (abbreviated as CIELAB). Then, lower-degree polynomial regression is employed to eliminate color errors due to the mismatch between spectral response functions. Experimental results indicate that the root-mean-square* $\Delta E^*_{ab}$ *value (i.e., color error) from the degree-3 polynomial regression is less than a just-noticeable difference (about 2.3) in CIELAB. It appears that the proposed technique can establish an accurate colorimetric model for vision systems.* © *2000 SPIE and IS&T.*
[S1017-9909(00)01604-4]

## 1 Introduction

For many years, it has been broadly recognized that the use of color becomes increasingly significant in a variety of fields, such as visualization and image rendering, machine vision, pattern recognition, and so on. Specifically, a realistic image is a projection from a scene onto a plane with sensor array(s), where it is digitized into discrete pixel positions and intensities through separating color signals. As a result, many imaging or vision systems are purposely designed to be capable of using color as a feature for object recognition, or of rendering (or synthesizing) scene images with computer generated imagery to meet commercial or specific needs. Evidently, it is extremely desirable to enable these systems to have the ability of color perception analogous to that of human beings.

For objectively describing color sensations, colorimetry has played a prominent role in characterizing incident light spectrum with the help of a set of numbers named tristimulus values. Unfortunately, in practice, the color accuracy of vision systems are highly restricted, even though several international standards have been established, e.g., International Commission on Illumination (CIE) recommendations in colorimetry, National Television System Committee (NTSC) color standards, and so on.[1] There are several important factors resulting in color distortions, such as spectral imperfection of optical components, camera noise, and limitations in fabrication of color filters. For instance, chromatic aberration in a camera's lens geometrically projects the color channels [e.g., red-green-blue (RGB) channels] differently and as a consequence, misregistration between these channels brings about image color discrepancy.[2] Usually, the appearance of color from an imaging process is somewhat device-dependent or noncolorimetric. Therefore, the realization of device-independent color is still an essential issue, and we commonly call the color acquired from a vision system, device color.

Many researchers have devoted themselves to developing techniques for color characterization of imaging or vision devices, such as scanners and cameras.[1–16] Given the spectral reflectances, Vrhel and Trussell[3] proposed a method to correct device colors based on principle-component analysis. Jackowski *et al.*[2] presented an idea of lookup table mapping to reduce color errors. They determined three transformation functions using a number of image colors whose true (or colorimetric) values were measured. These functions were then used to estimate the measured value of each color in an image. Herzog *et al.*[7] used higher-degree polynomial regression method for color characterization. In this approach, since polynomials are global functions, these functions diminish local color errors over a specified color space. However, the color errors evaluated in this method should be minimized with a perceptual color difference measure, e.g., $\Delta E^*_{ab}$ in CIELAB space. Chang and Reid[12] introduced a color calibration method for eliminating the variations in RGB values caused by vision systems. In their approach, they suppose that color errors arise from gray-level shift, a variation in amplification and quantization in camera electronics or frame grabber, and so on. Usually, the severity of this problem is device dependent. In general, if the operation of a vision system can be accurately represented by a parametric color model, the characterization is readily done by determining the model parameters from a few measurements. As no analytic model is available, a pure empirical approach using a great amount of color samples is necessary, in which the characterization function is directly measured over a grid of specified data;[1]

*Author to whom correspondence should be addressed; Tel: +886-3-5731153; Fax: +886-3-5715971; E-mail: ycchen@ee.nthu.edu.tw

Paper 16-004 received Dec. 7, 1999; accepted for publication Apr. 26, 2000.
1017-9909/2000/$15.00 © 2000 SPIE and IS&T.

otherwise, color discrepancies will mislead the vision system. Therefore, it is very crucial to give a color imaging model for vision systems.

In this article, a colorimetric modeling technique is proposed not only to characterize device colors but also to develop a computational model, so that they are related to true (or measured) values. Specifically, this technique is to give better estimates of colorimetric values (e.g., CIE $L^*a^*b^*$ values) from electronic cameras. For this, we first estimate the camera spectral responses, from the principle of color image formation (i.e., spectral integration), under reasonable assumptions. The determination of spectral responsivities is essential since these responses reflect variations in the imaging parameters, such as aperture stop size and white balance setting, which considerably influence the performance of color imaging. Then, we assess the colorimetric quality for the camera imaging system to examine the feasibility of colorimetric modeling. Specifically, the measure of colorimetric quality introduced by Neugebauer,[17] called $q$ factor, can be computed from the spectral characteristics, and it theoretically reveals the degree of the correlation between device colors and CIE tristimulus values for human vision. This factor also indicates the potential capability of an imaging device to give meaningful color representations, to some extent, in connection with colorimetry.

In our approach, the colorimetric modeling process involves three major steps in the following. First, we introduce a spectral matching method for computing device colors with a set of synthesized spectral responsivities, which are optimally matched to standardized spectral response functions, e.g., NTSC-RGB standard,[18] in the least-squares sense, from the camera's spectral features. Second, we present an approach to determining a reference-white luminance so that the device colors and true (or measured) colors can be well coordinated, with regard to the strength of a global illumination or display white, in a perceptually uniform color space, e.g., CIE 1976 $L^*a^*b^*$ space[19] (CIELAB). Third, the polynomial regression technique is employed to eliminate color errors due to the mismatch between spectral response functions. These three methods are formulated by individually specified functions. Then, these functions are incorporated with the spectral integration form for camera imaging, and consequently the colorimetric model for vision systems is established.

In our experiments, a color testing and measurement scheme based on the CIE 0/45 configuration[19] is developed. By using multiple polynomial regression for color correction, it is found that as the degree of polynomial increases from 1 to 2, the root-mean-square (rms) $\Delta E^*_{ab}$ value dramatically decreases. This implies that the methods of spectral matching and evaluating reference-white luminance are essential and effective. That is, only lower-degree polynomial regression is needed to eliminate residual color errors. Experimental results indicate that the rms $\Delta E^*_{ab}$ values from the degree-3 polynomial regression are sufficiently small in CIELAB, since they are less than a just-noticeable difference[1] (about 2.3 $\Delta E^*_{ab}$ unit).

This article is organized as follows. Section 2 describes the mathematical model of color imaging. Section 3 presents the colorimetric quality evaluation. The colorimetric modeling technique is introduced in Sec. 4, and detailed derivations for the spectral matching method are left to Appendix A. Also, color coordinate transformations are formulated in Appendix B. Section 5 gives the experimental results. Finally, Sec. 6 concludes this article.

## 2 Mathematical Model of Color Imaging

### 2.1 *Camera Model*

A video camera with an objective lens is commonly capable of forming a color image by focusing light on its sensor array(s) and by separating color signals. It is reasonably assumed that no blooming occurs in imaging process and nonlinearities due to gamma correction (i.e., predistortion compensating for display phosphor properties) are not present. Over a restricted region, we may also ignore the spatial variations in incident light with spectral power distribution $C(\lambda)$ of wavelength $\lambda$ and the spatial nonuniformities of camera's spectral responsivities $S^{(k)}(\lambda)$ of color channels, $k=1, 2, 3$. Therefore, at a given time instant, the imaging process can be modeled[4,14] as

$$u^{(k)}=\int_{\lambda_1}^{\lambda_2} C(\lambda)S^{(k)}(\lambda)d\lambda+\beta^{(k)}+n^{(k)}, \tag{1}$$

where the spatial average values $u^{(k)}$, $\beta^{(k)}$, and $n^{(k)}$ represent the camera output, bias value due to dark current, and camera noise of the $k$th channel, respectively. Usually, the practical visible range $[\lambda_1,\lambda_2]=[400\text{ nm}, 700\text{ nm}]$ and the color channels, $k=1, 2, 3$, are designated for the red, green, and blue (RGB) channels. In Eq. (1), we consider that the values of $\beta^{(k)}$, $k=1, 2, 3$, are constant and the image sensor(s) is less sensitive to change in temperature. Evidently, these values can be obtained by taking the average of repeated outputs of camera imaging with no incident light if the mean value of camera noise is generally assumed to be zero. Furthermore, parameters of camera imaging, such as size of aperture stop, the setting value of white balance, and so on, are supposed to be fixed since the spectral responsivities are influenced by these parameters.

### 2.2 *Estimation of Spectral Responsivities*

To estimate camera's spectral responses, we develop a filter-based optical system, as shown in Fig. 1. The optical system primarily consists of a diffused area light source, a collection of spectral filters mounted on a rotary wheel, and a platform for shielding the light source from ambient light. In Fig. 1, the surfaces of these spectral (or color) filters with spectral transmittances $\{F_i(\lambda),\ i=1,\ 2,...,\ N_C\}$, where $N_C$ is the number of the filters, are parallel to that of the light source with spectral power distribution $I(\lambda)$. As a result, the light ray from the radiation source going, in sequence, through these filters generates a collection of colored light, called color stimuli, $\{C_i(\lambda),\ i=1,\ 2,...,\ N_C\}$. That is, we have

$$C_i(\lambda)=F_i(\lambda)I(\lambda),\ \ i=1,\ 2,...,\ N_C. \tag{2}$$

In the optical system, the color stimuli individually incident upon a digital camera under test are used to excite

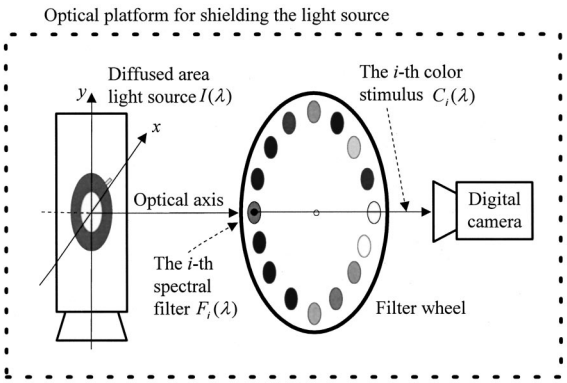


**Fig. 1** Filter-based optical system for estimating spectral responsivities.

the features of color imaging so that the spectral characteristics can be truly extracted from observations. From Eq. (1), we have

$$u_i^{(k)} = \int_{\lambda_1}^{\lambda_2} C_i(\lambda) S^{(k)}(\lambda) d\lambda + \beta^{(k)} + n_i^{(k)}, \tag{3}$$

where $u_i^{(k)}$ means the camera output and $n_i^{(k)}$ is the camera noise, for the $k$th channel, in response to the $i$th color stimulus $C_i(\lambda)$. In general, Eq. (3) can be approximated in vector forms, with quadrature sampling, i.e.,

$$\tilde{u}_i^{(k)} = (\mathbf{C}_i)^{\mathrm{T}} \mathbf{S}^{(k)} + n_i^{(k)}, \quad i = 1, 2, ..., N_C, \text{ and } k = 1, 2, 3, \tag{4}$$

where $\tilde{u}_i^{(k)} = u_i^{(k)} - \beta^{(k)}$ is a trimmed observation, $\mathbf{S}^{(k)}$ and $\mathbf{C}_i$ are $N_W \times 1$ column vectors of quadrature samples for representing $S^{(k)}(\lambda)$ and $C_i(\lambda)$, respectively, with the sampling interval $\Delta\lambda_S$ and the number of quadrature samples $N_W$, and the superscript T means matrix (or vector) transpose. Obviously, the number of the color stimuli, $N_C$, must be larger than or equal to $N_W$ for estimating $\mathbf{S}^{(k)}$. Thus, let $N_W = N_C$ for computational convenience.

From Eq. (4), the set of trimmed observations, $\{\tilde{u}_i^{(k)}, i = 1, 2, ..., N_C\}$, corresponding to these color stimuli can be arranged in the $N_C \times 1$ vector

$$\tilde{\mathbf{U}}^{(k)} = \mathbf{C}\mathbf{S}^{(k)} + \mathbf{n}^{(k)}, \quad k = 1, 2, 3, \tag{5}$$

where the vector $(\mathbf{C}_i)^{\mathrm{T}}$ occupies the $i$th row of the matrix $\mathbf{C} \in \boldsymbol{R}^{\mathrm{N_C} \times \mathrm{N_C}}$ and $\mathbf{n}^{(k)} \in \boldsymbol{R}^{\mathrm{N_C} \times 1}$ is the $k$th channel noise vector from $N_C$ observations. Obviously, the vectors $\mathbf{S}^{(k)} \in \boldsymbol{R}^{\mathrm{N_C} \times 1}$, $k = 1, 2, 3$, for spectral responsivities in Eq. (5) can be estimated if

$$\mathrm{rank}(\mathbf{C}) = N_C, \tag{6}$$

where the computation of matrix rank is denoted as rank $(\cdot)$. Moreover, it can be shown that the matrix $\mathbf{C}$ must be well-conditioned to achieve satisfactory estimation accuracy;[20] that is, the solution vector for Eq. (5) can be less sensitive to camera noise.

Physically, the elements in the spectral vectors $\{\mathbf{S}^{(k)}, k = 1, 2, 3\}$, i.e., the spectral values, are supposed to be all non-negative. We denote this constraint as

$$\mathbf{S}^{(k)} \geqslant 0, \quad k = 1, 2, 3. \tag{7}$$

To solve Eq. (5) for the optimal solution vectors $\{\hat{\mathbf{S}}^{(k)}, k = 1, 2, 3\}$ in the least squares sense, we adopt a nonnegative least-squares (NNLS) algorithm proposed by Lawson and Hanson,[21] for the NNLS problem as follows:

Problem NNLS:

$$\text{Minimize} \left\| \mathbf{C}\mathbf{S}^{(k)} - \tilde{\mathbf{U}}^{(k)} \right\|_2,$$

$$\text{subject to } \mathbf{S}^{(k)} \geqslant 0, \quad k = 1, 2, 3, \tag{8}$$

where $\mathbf{C} \in \boldsymbol{R}^{\mathrm{N_C} \times \mathrm{N_C}}$, the estimates $\{\hat{\mathbf{S}}^{(k)}, k = 1, 2, 3\}$ of $\mathbf{S}^{(k)}$ and the trimmed observations $\{\tilde{\mathbf{U}}^{(k)}, k = 1, 2, 3\}$ are all $N_C \times 1$ vectors, and $\|\cdot\|_2$ denotes the 2-norm for a vector.[20] Furthermore, from the estimated vectors $\{\hat{\mathbf{S}}^{(k)}, k = 1, 2, 3\}$, one can use an interpolation technique, such as a low-pass filtering technique for perfect reconstruction,[22] to obtain interpolated vectors $\{\hat{\tilde{\mathbf{S}}}^{(k)}, k = 1, 2, 3\}$ for representing the estimated spectral responsivities $\hat{\tilde{S}}^{(k)}(\lambda)$, $k = 1, 2, 3$, with a desired wavelength resolution.

## 3 Colorimetric Quality Evaluation

It is well known that the spectral responsivities highly influence the color imaging performance. The evaluation of colorimetric quality for an imaging device means to measure the degree of how closely its spectral responsivities correspond to those of the human eye. For this, the Luther–Ives condition[17] plays a significant role in the link between device colors and human vision. It states that visually identical colors will be photographed identically if the spectral sensitivities (or responsivities) conform to any set of color-mixture curves. A color-mixture curve, denoted as $O(\lambda)$, can be derived from

$$O(\lambda) = \alpha_1 \overline{x}(\lambda) + \alpha_2 \overline{y}(\lambda) + \alpha_3 \overline{z}(\lambda), \tag{9}$$

where $\alpha_1$, $\alpha_2$, and $\alpha_3$ are all real numbers and $\overline{x}(\lambda)$, $\overline{y}(\lambda)$, and $\overline{z}(\lambda)$ are the color matching functions (CMFs) of the CIE 1931 $(X, Y, Z)$ system.[19] These functions are called CIE$XYZ$ color-matching functions and in Fig. 2, they are depicted and labeled CMFs $x$, $y$, and $z$, respectively.

Based on this crucial fact, Neugebauer[17] introduced colorimetric quality factors, called $q$ factors, to describe how closely spectral responsivities of an imaging device match color-mixture curves, which ensure that visually identical colors will reproduce alike. To calculate $q$ factors, he suggested a set of orthogonal color-mixture curves, denoted as $\{O_1(\lambda), O_2(\lambda), O_3(\lambda)\}$, as specified below

$$O_1(\lambda) = -0.4066\overline{x}(\lambda) + 0.5521\overline{y}(\lambda), \tag{10a}$$

$$O_2(\lambda) = 0.4066\overline{x}(\lambda) - 0.0433\overline{y}(\lambda), \tag{10b}$$

and

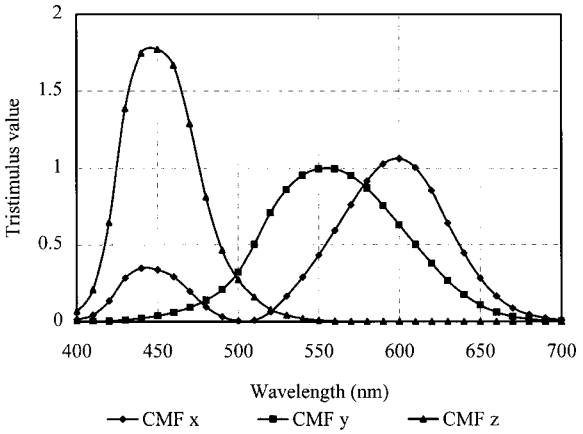


**Fig. 2** Color matching functions of CIE 1931 ($X, Y, Z$) system.

$$O_3(\lambda) = -0.179\overline{x}(\lambda) + 0.1018\overline{y}(\lambda) + 0.281\overline{z}(\lambda). \quad (10c)$$

As a consequence, given the estimated spectral responsivities $\hat{S}^{(k)}(\lambda)$, the colorimetric quality factors $q^{(k)}$ of a camera, for color channels $k=1,\ 2,\ 3$, can be defined by

$$q^{(k)} = \sum_{i=1}^{3} [(\hat{\mathbf{S}}^{(k)})^T \mathbf{O}_i]^2 / [(\hat{\mathbf{S}}^{(k)})^T (\hat{\mathbf{S}}^{(k)})], \quad (11)$$

where the column vector $\hat{\mathbf{S}}^{(k)}$ represents $\hat{S}^{(k)}(\lambda)$ with a desired wavelength resolution $\Delta\lambda_d$ and the column vector $\mathbf{O}_i$ stands for the orthogonal color-mixture curve $O_i(\lambda)$, $i=1,\ 2,\ 3$, from Eqs. (10a)–(10c), with the same resolution $\Delta\lambda_d$. Obviously, the value of $q$ factor ranges from zero to one, and in particular, it is equal to one for an exact color-mixture curve. That is, the spectral responsivities of a camera can closely match color-mixture curves as the $q$ factors approach one.

## 4 Colorimetric Modeling Technique

As indicated in Sec. 3, color-mixture curves are central to evaluating colorimetric quality. From Eq. (9), it is obvious that the number of color-mixture curves is infinite because they are obtained by linear combinations of the CIE$XYZ$ color-matching functions. The NTSC-RGB standard has been broadly recognized and utilized in video systems and television industry. Its spectral responsivities with a specified reference white can be derived from those color-matching functions, according to the chromaticity coordinates of display phosphor primaries. Evidently, these spectral responses are color-mixture curves since their colorimetric quality factors are all equal to 1. In addition, from various colorimetric investigations,[18] there is a tendency to use a daylight-type illuminant with correlated color temperature (CCT) 6500 K as a reference white, e.g., the CIE recommended illuminant $D_{65}$. Thus, without loss of generality, we adopt the NTSC-RGB spectral responsivities with illuminant $D_{65}$ as a set of representative color-mixture curves. Also, for convenience of color error assessment, we assume that colored light incident upon a video camera can be represented in the reproducible gamut of the NTSC-RGB standard.

### 4.1 *Computing Device Colors with Spectral Matching*

Ideally, from the Luther–Ives condition, one can see that the colorimetric quality is perfect (i.e., all $q$ factors for color channels equal to 1) if a set of linear combinations of camera's spectral responsivities exactly conform to the NTSC-RGB spectral responsivities. In matrix forms, it appears that

$$\mathbf{A}_S \mathbf{M}_S = [\mathbf{R}_N\ \mathbf{G}_N\ \mathbf{B}_N], \quad (12)$$

where $\mathbf{A}_S = [\mathbf{R}_S\ \mathbf{G}_S\ \mathbf{B}_S] \in \boldsymbol{R}^{N_S \times 3}$ is composed of the column vectors that stand for the camera spectral responses $R_S(\lambda)$, $G_S(\lambda)$, and $B_S(\lambda)$ with sample number $N_S$, which are referred to as the estimated spectral responsivities, $\hat{S}^{(k)}(\lambda)$, $k=1,\ 2,\ 3$, from Sec. 2.2, respectively; also $\mathbf{M}_S = [\mathbf{m}_1\ \mathbf{m}_2\ \mathbf{m}_3]$ consists of the column vectors $\mathbf{m}_i \in \boldsymbol{R}^{3\times 1}$, $i=1,\ 2,\ 3$, and $\mathbf{R}_N$, $\mathbf{G}_N$, and $\mathbf{B}_N \in \boldsymbol{R}^{N_S \times 1}$ individually represent the NTSC-RGB spectral responsivities, denoted as $R_N(\lambda)$, $G_N(\lambda)$, and $B_N(\lambda)$, with the same number $N_S$.

The spectral imperfections of a camera make it necessary to find a least-squares solution. This solution, denoted as $\hat{\mathbf{m}}_i \in \boldsymbol{R}^{3\times 1}$, $i=1,\ 2,\ 3$, for Eq. (12), can be readily obtained, e.g., $\hat{\mathbf{m}}_1 = (\mathbf{A}_S^T \mathbf{A}_S)^{-1} \mathbf{A}_S^T \mathbf{R}_N$. As a result, the synthesized (or matched) spectral responsivities $R_C(\lambda)$, $G_C(\lambda)$, and $B_C(\lambda)$ can be expressed as

$$[\mathbf{R}_C\ \mathbf{G}_C\ \mathbf{B}_C]^{\mathrm{T}} = \hat{\mathbf{M}}_S^{\mathrm{T}} \mathbf{A}_S^{\mathrm{T}} = \hat{\mathbf{M}}_S^{\mathrm{T}} [\mathbf{R}_S\ \mathbf{G}_S\ \mathbf{B}_S]^{\mathrm{T}}, \quad (13)$$

where $\hat{\mathbf{M}}_S = [\hat{\mathbf{m}}_1\ \hat{\mathbf{m}}_2\ \hat{\mathbf{m}}_3]$ and the column vectors $\mathbf{R}_C$, $\mathbf{G}_C$, and $\mathbf{B}_C \in \boldsymbol{R}^{N_S \times 1}$ represent these matched spectral responses, respectively.

Now, let's compute device colors with the spectral matching, denoted as $(R_C^{(i)}, G_C^{(i)}, B_C^{(i)})$, in response to the $i$th testing colored light (TCL) $T_i(\lambda)$ incident upon the camera, for $i=1$ to $N_M$, where $N_M$ is the number of the testing light. The $i$th device color, represented as a vector $\mathbf{V}_C^{(i)} \in \boldsymbol{R}^{3\times 1}$, can be formulated as

$$\begin{aligned} \mathbf{V}_C^{(i)} &= [R_C^{(i)}\ G_C^{(i)}\ B_C^{(i)}]^{\mathrm{T}} \\ &= \hat{\mathbf{M}}_S^{\mathrm{T}} [(R_S^{(i)} - \beta_R)\ (G_S^{(i)} - \beta_G)\ (B_S^{(i)} - \beta_B)]^{\mathrm{T}}, \\ &\quad i = 1\ \text{ to }\ N_M, \end{aligned} \quad (14)$$

where $R_S^{(i)}$, $G_S^{(i)}$, and $B_S^{(i)}$ stand for the camera outputs from RGB channels, and $\beta_R$, $\beta_G$, and $\beta_B$ mean $\beta^{(k)}$, $k=1,\ 2,\ 3$, from Sec. 2.1 and Eq. (3), respectively. For details, please refer to Appendix A. In Eq. (14), the camera output subtracted from the bias value due to dark current, e.g., $\beta_R$, is called trimmed camera output, e.g., $R_S^{(i)} - \beta_R$. In addition, Appendix A gives detailed expressions to normalize the vector $\mathbf{V}_C^{(i)}$.

To distinguish the device colors from the camera outputs, we call $\mathbf{V}_C^{(i)}$ device-color vector, which represents the

device color computed with the trimming and spectral matching, and let $\mathbf{V}_S^{(i)}=[R_S^{(i)}\ G_S^{(i)}\ B_S^{(i)}]^{\mathrm{T}}\in\boldsymbol{R}^{3\times1}$ stand for the camera-output vector. From the computations of the spectral matching, trimming, and normalization, we define a function $\Phi_C(\cdot)$ that maps a camera-output vector onto a normalized device-color vector. That is, we have

$$\overline{\mathbf{V}}_C^{(i)}=\Phi_C(\mathbf{V}_S^{(i)}),\quad i=1\ \text{ to }\ N_M, \tag{15}$$

where $\mathbf{V}_S^{(i)}\in\boldsymbol{R}^{3\times1}$ is the camera-output vector and $\overline{\mathbf{V}}_C^{(i)}=[\overline{R}_C^{(i)}\ \overline{G}_C^{(i)}\ \overline{B}_C^{(i)}]^{\mathrm{T}}\in\boldsymbol{R}^{3\times1}$ means the normalized device-color vector, in response to the $i$th incident light $T_i(\lambda)$.

### 4.2 *Determining Reference-White Luminance*

For the link between the device colors and the measured colors [e.g., the colorimetric data of the $i$th incident light $T_i(\lambda)$], it is essential to determine the reference-white luminance, denoted as $Y_0$, since the color image data acquired from a digital camera can hardly give a physical quantity of luminance. To tackle this problem, the basic idea is to estimate $Y_0$ so that the chromaticity coordinates and luminances of the device colors correspond to those of the measured colors as closely as possible in CIELAB space. In other words, it is to minimize the color errors between the device colors and the measured colors with a reference-white luminance to be determined.

To represent device colors in CIELAB, we consider the following two color coordinate transformations. First, for the $i$th normalized vector $\overline{\mathbf{V}}_C^{(i)}=[\overline{R}_C^{(i)}\ \overline{G}_C^{(i)}\ \overline{B}_C^{(i)}]^{\mathrm{T}}\in\boldsymbol{R}^{3\times1}$, the transformation from NTSC-RGB (with illuminant $D_{65}$) to CIE$XYZ$ can be expressed as a function $\Phi_X(\cdot)$, i.e.,

$$\overline{\mathbf{V}}_X^{(i)}=\Phi_X(\overline{\mathbf{V}}_C^{(i)})=[\overline{X}_C^{(i)}\ \overline{Y}_C^{(i)}\ \overline{Z}_C^{(i)}]^{\mathrm{T}},\quad i=1\ \text{ to }\ N_M, \tag{16}$$

where $\overline{\mathbf{V}}_X^{(i)}\in\boldsymbol{R}^{3\times1}$ is the device-color vector in CIE$XYZ$. For details, please refer to Appendix B.

Second, the transformation from CIE$XYZ$ coordinate (or tristimulus values) $(X,Y,Z)$ to CIELAB coordinate $(L^*,a^*,b^*)$ can be found in Appendix B. It is noted that asterisks of conventional use in literature for CIELAB coordinates may be omitted here for notational simplicity. Similar to Eq. (16), this transformation can be also expressed as a function $\Phi_L(\cdot)$. Then, we have the vector

$$\mathbf{V}_L^{(i)}=\Phi_L(\overline{\mathbf{V}}_X^{(i)})=[L_C^{(i)}\ a_C^{(i)}\ b_C^{(i)}]^{\mathrm{T}},\quad i=1\ \text{ to }\ N_m, \tag{17}$$

where $\mathbf{V}_L^{(i)}\in\boldsymbol{R}^{3\times1}$ is the device-color vector in CIELAB and $\overline{\mathbf{V}}_X^{(i)}=[\overline{X}_C^{(i)}\ \overline{Y}_C^{(i)}\ \overline{Z}_C^{(i)}]^{\mathrm{T}}\in\boldsymbol{R}^{3\times1}$. In this transform, since the color coordinate $(x_0,y_0,z_0)$ of illuminant $D_{65}$ equals (0.3127, 0.3291, 0.3582), we have its tristimulus values in CIE$XYZ$

$$\begin{aligned}(X_0,Y_0,Z_0)&=((x_0/y_0)Y_0,Y_0,(z_0/y_0)Y_0)\\&=(0.9502Y_0,Y_0,1.088Y_0).\end{aligned} \tag{18}$$

Now, we intend to minimize the root-mean-square (rms) color error in CIELAB space,

$$\text{rms}\,\Delta E_{\text{ab}}^*=\left[\frac{1}{N_M}\sum_{i=1}^{N_M}(\Delta E_{\text{ab}}^{(i)})^2\right]^{1/2}, \tag{19}$$

and

$$\begin{aligned}\Delta E_{\text{ab}}^{(i)}=[&(L_C^{(i)}-L_M^{(i)})^2+(a_C^{(i)}-a_M^{(i)})^2\\&+(b_C^{(i)}-b_M^{(i)})^2]^{1/2},\end{aligned} \tag{20}$$

for $i=1,\ 2,...,\ N_M$,

where $(L_M^{(i)},a_M^{(i)},b_M^{(i)})$ is the CIELAB coordinate of the $i$th measured color. From Appendix B and Eqs. (16)–(18), given the normalized tristimulus values $(\overline{X}_C^{(i)},\overline{Y}_C^{(i)},\overline{Z}_C^{(i)})$ and measured ones $(X_M^{(i)},Y_M^{(i)},Z_M^{(i)})$, $i=1,\ 2,...,\ N_M$, in CIE$XYZ$, we can see that $\Delta E_{\text{ab}}^*$ is the function of only the unknown variable $Y_0$. It appears that the solution of $Y_0$ for minimizing $\text{rms}\,\Delta E_{\text{ab}}^*$ can be obtained by using optimization techniques or by means of numerical calculations. Once the reference-white luminance is determined, the device and measured color coordinates $(L_C^{(i)},a_C^{(i)},b_C^{(i)})$ and $(L_M^{(i)},a_M^{(i)},b_M^{(i)})$, $i=1,\ 2,...,\ N_M$, in CIELAB are obtained.

### 4.3 *Color Correction Using Multiple Polynomial Regression*

So far, the device colors and measured colors have been well coordinated, with the above evaluated strength of a global illumination (or display white), i.e., the computed $Y_0$, in CIELAB. To eliminate the remaining color errors between them, we employ the technique of multiple polynomial regression. Specifically, we use this technique for the color correction since the colorimetric quality factors are usually less than 1. The polynomial, of variables $L_C$, $a_C$, and $b_C$, with degree $j$ can be formulated as

$$p_j(L_C,a_C,b_C)=(\mathbf{p}_j)^{\mathrm{T}}\mathbf{k}_j, \tag{21}$$

where $\mathbf{p}_j$ is a column vector of the polynomial, $\mathbf{k}_j$ is a column vector of its associated coefficient, and $j$ is a nonnegative integer. Table 1 lists the corresponding column vectors $\mathbf{p}_j$ and $\mathbf{k}_j$, for $j=0,\ 1,\ 2,\ 3$. We select several representative terms for the polynomials with the degree ranging from 0 to 3. Although they are not complete, we just intend to verify the effectiveness of color correction using polynomial regression with a certain degree. This is because, as the degree of the polynomial increases, the residual color error will theoretically decrease.

Since the three components, $L^*$, $a^*$, and $b^*$, of CIELAB coordinates are mutually independent, we may formulate the problem of color error minimization (i.e., color correction) in terms of these components, respectively. For instance, regarding the $L^*$ components of all the device and measured color coordinates $(L_C^{(i)},a_C^{(i)},b_C^{(i)})$ and $(L_M^{(i)},a_M^{(i)},b_M^{(i)})$, $i=1,\ 2,...,\ N_M$, in CIELAB, we can obtain the solution vector $\hat{\mathbf{k}}_{j(L)}$, such that

$$\|\mathbf{P}_j\mathbf{k}_{j(L)}-\mathbf{L}_M\|_2\ \text{ is minimized}, \tag{22}$$

**Table 1** Polynomial vector and its associated coefficient vector.

| Polynomial type | Polynomial vector and its associated coefficient vector |
|---|---|
| Degree zero (or constant) | $\mathbf{p}_0=1,\ \mathbf{k}_0=k_0$ |
| Degree 1 | $\mathbf{p}_1=[1\ L_C\ a_C\ b_C]^{\mathrm{T}},\ \mathbf{k}_1=[k_0\ k_{11}\ k_{12}\ k_{13}]^{\mathrm{T}}$ |
| Degree 2 | $\mathbf{p}_2=[1\ L_C\ a_C\ b_C\ L_C^2\ a_C^2\ b_C^2\ L_Ca_C\ L_Cb_C\ a_Cb_C]^{\mathrm{T}}$<br>$\mathbf{k}_2=[k_0\ k_{11}\ k_{12}\ k_{13}\ k_{21}\ k_{22}\ k_{23}\ k_{24}\ k_{25}\ k_{26}]^{\mathrm{T}}$ |
| Degree 3 | $\mathbf{p}_3=[1\ L_C\ a_C\ b_C\ L_C^2\ a_C^2\ b_C^2\ L_Ca_C\ L_Cb_C\ a_Cb_C\ L_C^3\ a_C^3\ b_C^3\ L_Ca_Cb_C]^{\mathrm{T}}$<br>$\mathbf{k}_3=[k_0\ k_{11}\ k_{12}\ k_{13}\ k_{21}\ k_{22}\ k_{23}\ k_{24}\ k_{25}\ k_{26}\ k_{31}\ k_{32}\ k_{33}\ k_{34}]^{\mathrm{T}}$ |

where $\mathbf{P}_j=[\mathbf{p}_j^{(1)}\ \mathbf{p}_j^{(2)}\ldots\mathbf{p}_j^{(N_M)}]^{\mathrm{T}}$, $\mathbf{L}_M=[L_M^{(1)}\ L_M^{(2)}\ldots L_M^{(N_M)}]^{\mathrm{T}}$, and $\mathbf{p}_j^{(i)}$ means the column vector $\mathbf{p}_j$ with $(L_C,a_C,b_C)=(L_C^{(i)},a_C^{(i)},b_C^{(i)})$, as defined in Table 1, e.g., $\mathbf{p}_1^{(i)}=[1\ L_C^{(i)}\ a_C^{(i)}\ b_C^{(i)}]^{\mathrm{T}}$. As a consequence, the column vector representing the $L^*$ components of the corrected device colors is expressed as

$$\hat{\mathbf{L}}_C=[\hat{L}_C^{(1)}\ \hat{L}_C^{(2)}\ldots\hat{L}_C^{(N_M)}]^{\mathrm{T}}=\mathbf{P}_j\hat{\mathbf{k}}_{j(L)}, \tag{23}$$

where $\hat{\mathbf{k}}_{j(L)}=(\mathbf{P}_j^{\mathrm{T}}\mathbf{P}_j)^{-1}\mathbf{P}_j^{\mathrm{T}}\mathbf{L}_M$.

Likewise, we can obtain the column vectors $\hat{\mathbf{a}}_C=[\hat{a}_C^{(1)}\ \hat{a}_C^{(2)}\ldots\ \hat{a}_C^{(N_M)}]^{\mathrm{T}}=\mathbf{P}_j\hat{\mathbf{k}}_{j(a)}$ and $\hat{\mathbf{b}}_C=[\hat{b}_C^{(1)}\ \hat{b}_C^{(2)}\ldots\ \hat{b}_C^{(N_M)}]^{\mathrm{T}}=\mathbf{P}_j\hat{\mathbf{k}}_{j(b)}$ for the $a^*$ and $b^*$ components of the corrected device colors, where $\hat{\mathbf{k}}_{j(a)}$ and $\hat{\mathbf{k}}_{j(b)}$ are the solution vectors for the error minimization problem of $a^*$ and $b^*$ components, similar to that for $\hat{\mathbf{k}}_{j(L)}$ in Eq. (22). It appears that the color errors between $(L_C^{(i)},a_C^{(i)},b_C^{(i)})$ and $(L_M^{(i)},a_M^{(i)},b_M^{(i)})$, $i=1,\ 2,...,\ N_M$, will be minimal through the polynomial regression technique with a specified degree.

Therefore, we can define a function $\Phi_{P(j)}(\cdot)$ to stand for the degree-$j$ polynomial regression, which maps the device-color vector $\mathbf{V}_L^{(i)}=[L_C^{(i)}\ a_C^{(i)}\ b_C^{(i)}]^{\mathrm{T}}\in\boldsymbol{R}^{3\times1}$ onto the corrected one $\hat{\mathbf{V}}_L^{(i)}=(\hat{L}_C^{(i)},\hat{a}_C^{(i)},\hat{b}_C^{(i)})$, i.e.,

$$\hat{\mathbf{V}}_L^{(i)}=\Phi_{P(j)}(\mathbf{V}_L^{(i)}),\quad \text{for } i=1 \text{ to } N_M. \tag{24}$$

### 4.4 *Colorimetric Imaging Model*

The process of colorimetric modeling is briefly reviewed in the following and its flow diagram is shown in Fig. 3:
Step 1: Trimming and normalizing camera outputs [from Eqs. (A3) and (A4) in Appendix A],

denoted as

$$(R_S^{(i)},G_S^{(i)},B_S^{(i)})\rightarrow(\overline{R}_S^{(i)},\overline{G}_S^{(i)},\overline{B}_S^{(i)}),\ \text{for } i=1 \text{ to } N_M;$$

Step 2: Computing device colors with the spectral matching,

$$(\overline{R}_S^{(i)},\overline{G}_S^{(i)},\overline{B}_S^{(i)})\rightarrow(\overline{R}_C^{(i)},\overline{G}_C^{(i)},\overline{B}_C^{(i)}),\ \text{for } i=1 \text{ to } N_M;$$

Step 3: Transforming the NTSC-RGB coordinates to those of CIE$XYZ$, i.e.,

$$(\overline{R}_C^{(i)},\overline{G}_C^{(i)},\overline{B}_C^{(i)})\rightarrow(\overline{X}_C^{(i)},\overline{Y}_C^{(i)},\overline{Z}_C^{(i)}),\ \text{for } i=1 \text{ to } N_M;$$

Step 4: Collecting the measured colorimetric data of TCL, i.e., color coordinates $(x_M^{(i)},y_M^{(i)},Y_M^{(i)})$ or tristimulus values $(X_M^{(i)},Y_M^{(i)},Z_M^{(i)})$, and transforming the CIE$XYZ$ data $(X_M^{(i)},Y_M^{(i)},Z_M^{(i)})$ and $(\overline{X}_C^{(i)},\overline{Y}_C^{(i)},\overline{Z}_C^{(i)})$ to the coordinates of CIELAB with the reference-white luminance to be determined, i.e.,

$$(X_M^{(i)},Y_M^{(i)},Z_M^{(i)})\rightarrow(L_M^{(i)},a_M^{(i)},b_M^{(i)})$$

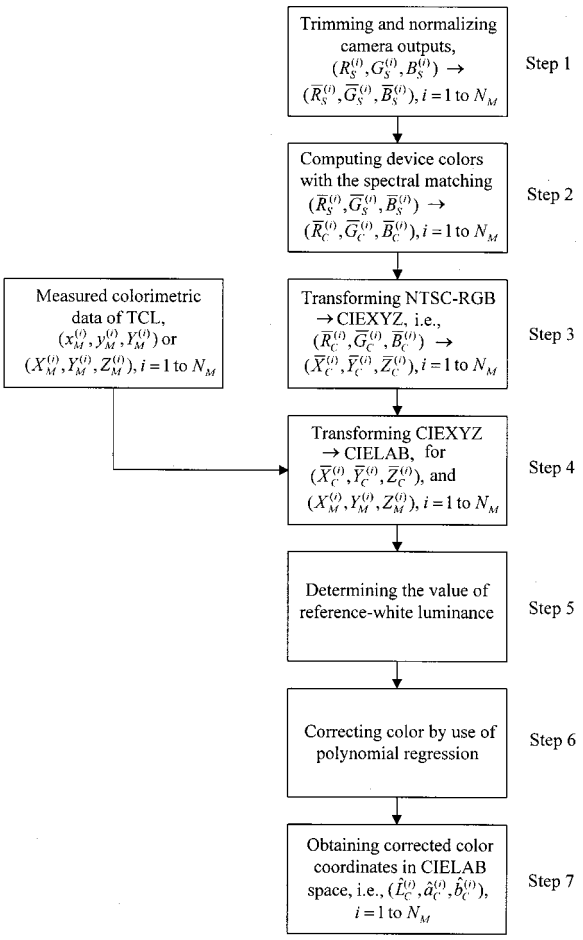


**Fig. 3** Flow diagram of colorimetric modeling process.

and

$$(\overline{X}_C^{(i)},\overline{Y}_C^{(i)},\overline{Z}_C^{(i)})\rightarrow(L_C^{(i)},a_C^{(i)},b_C^{(i)}),\ \text{for}\ i=1\ \text{to}\ N_M;$$

Step 5: Determining the value of reference-white luminance;
Step 6: Correcting color by use of polynomial regression;
Step 7: Obtaining corrected color coordinates in CIELAB space, denoted as $(\hat{L}_C^{(i)},\hat{a}_C^{(i)},\hat{b}_C^{(i)})$, for $i=1$ to $N_M$.

In summary, the colorimetric model for camera imaging can be expressed as

$$\hat{\mathbf{V}}_L=\Phi_{P(j)}[\Phi_L\{\Phi_X[\Phi_C(\mathbf{V}_S)]\}], \tag{25}$$

where $\Phi_C(\cdot)$, $\Phi_X(\cdot)$, $\Phi_L(\cdot)$, and $\Phi_{P(j)}(\cdot)$ are individually defined in Eqs. (15)–(17), and (24), $\mathbf{V}_S=[R_S\ G_S\ B_S]^{\mathrm{T}}\in\boldsymbol{R}^{3\times1}$ is a camera-output vector in response to the incident light, and $\hat{\mathbf{V}}_L=[\hat{L}_C\ \hat{a}_C\ \hat{b}_C]^{\mathrm{T}}\in\boldsymbol{R}^{3\times1}$ is the corrected device-color vector in CIELAB space. Since the coordinate transformations $\Phi_X(\cdot)$ and $\Phi_L(\cdot)$ are both one-to-one mappings, we may take their inverses $\Phi_X^{-1}(\cdot)$ and $\Phi_L^{-1}(\cdot)$ to obtain the desired representation of the corrected device-color vector for the need of applications in computer vision. For example, from Eq. (25), the corrected device-color vector in CIE*XYZ* or NTSC-RGB standard is represented as $\Phi_L^{-1}(\hat{\mathbf{V}}_L)$ or $\Phi_X^{-1}[\Phi_L^{-1}(\hat{\mathbf{V}}_L)]$ in response to the light incident upon the camera.

In Sec. 2, one sees that the camera imaging process is expressed as a mathematical model (i.e., a spectral integration form or a matrix form) with given (or estimated) spectral responsivities, under certain imaging conditions, from Eq. (1) or (5). Also, the functions $\Phi_C(\cdot)$, $\Phi_X(\cdot)$, $\Phi_L(\cdot)$, and $\Phi_{P(j)}(\cdot)$ can be entirely determined from this proposed modeling technique. Then, these functions are incorporated with the spectral integration form for camera imaging, and consequently the colorimetric model for vision systems is established. Therefore, we have a computational model for computer color vision.

## 5 Experimental Results

### 5.1 *Determining Spectral Responsivities and q Factors*

In the filter-based optical system, the diffused light source is operated at color correlated temperature (CCT) 5500 K and its spectral power distribution $I(\lambda)$ is exhibited in Fig. 4. To specify the number of spectral filters $N_C$, we suppose that the interval of quadrature sampling $\Delta\lambda_S=20$ nm is enough to characterize most spectral responsivity functions over the main visible region [410 nm, 690 nm]. The spectral responsivities over the remaining parts of the visible region, i.e., [400 nm, 410 nm] and [690 nm, 700 nm] can be readily obtained by the interpolation technique,[22] as mentioned in Sec. 2.2. Thus, we have $N_C=(690-410)/20=14$. The 14 spectral filters mounted on the rotary wheel are selected from a collection of Roscolux color filters, so that the condition from Eqs. (2) and (6) is satisfied for generating color stimuli. The spectral transmittances of these filters are shown in Figs. 5(a) and 5(b).

The color images from the 14 color stimuli were consecutively acquired and digitized by a Sony XC711 color camera (with a Cosmicar television lens) and a Matrox Meteor image grabber. The imaging parameters of the camera are all fixed in the experiment. For example, the shutter speed is set to 1/1000 second and the F-number equals 4 for the aperture stop of the lens. The digitized images that are represented by three 8-bit data for RGB channels, i.e., integer values ranging from 0 to 255, can be computed to obtain the corresponding camera output values. After removing the light source, we acquire an image from the camera with no incident light, and then the bias values $(\beta^{(1)},\beta^{(2)},\beta^{(3)})=(\beta_R,\beta_G,\beta_B)=(13,11,11)$ can be obtained from the image data. Thus, from Eqs. (4) and (5), the three $14\times1$ observation vectors $\tilde{\mathbf{U}}^k$, $k=1,\ 2,\ 3$, for RGB channels are constituted with the camera outputs and bias values, respectively.

From the NNLS method mentioned in Sec. 2.2, the spectral vectors $\{\hat{\mathbf{S}}^{(k)},\ k=1,\ 2,\ 3\}$ can be estimated. Also, we use the interpolation technique of low-pass filtering[22] to obtain the vector $\hat{\bar{\mathbf{S}}}^{(k)}$, interpolated from $\hat{\mathbf{S}}^{(k)}$, to represent the estimated spectral responsivities $\hat{\bar{S}}^{(k)}(\lambda)$, i.e., $R_S(\lambda)$, $G_S(\lambda)$, and $B_S(\lambda)$, with a desired wavelength resolution, e.g., 10 nm. Figure 6 exhibits the estimated spectral responsivities of the Sony XC711 color camera with a 10 nm wavelength resolution. The actual installation of the filter-based optical system is shown in Fig. 7.

To evaluate the colorimetric quality factors of this camera, the set of orthogonal color-mixture curves suggested by Neugebauer is used, as depicted in Fig. 8. Table 2 indicates the evaluation results of the $q$ factors and all of them exceed 0.85.

### 5.2 *Color Testing and Measurement (CTM) Scheme*

To characterize device colors, it is necessary to generate and measure a collection of testing light incident upon a digital camera. For this, based on the CIE 0/45 geometry measurement configuration,[19] a color testing and measurement scheme is presented, as illustrated in Fig. 9.

The light emanating from a tungsten halogen lamp (THL) with CCT 3200 K, which is housed in an iris diaphragm chamber, brings about directional illumination. The directional light illuminates the Macbeth ColorChecker (MCC) with the spot size of about one inch diameter and at a nonzero degree angle $\theta$ to the normal. In the 0/45 condition, the slight deviation, i.e., the angle $\theta$ not exceeding 10°, from strict normal illumination reduces the possibility of introducing systematic errors in the measurement caused by interreflections between samples that are not completely matte and the optical components that might be used to illuminate the sample.

The MCC with 24 color test patches is widely recognized to examine the color reproduction performance of various imaging devices, and thus it is qualified for the work of this scheme. In Fig. 9, the 24 patches of MCC, which is movable along the $x$ and $y$ axes, are individually illuminated by the incidence of the light source at an angle $\theta$ to the normal. At the same time, the 24 types of colored light are also reflected from the illuminated MCC patches at a 45° angle to the normal, respectively. The reflected

light is referred to as testing colored light (TCL) and labeled TCL Nos. 1–24, respectively.

In the similar fashion, as indicated in Fig. 9, we also use a daylight-type illuminant with about CCT 6500 K, called a $D_{65}$ illuminant, to generate additional 24 types of TCL. They are labeled TCL Nos. 25–48. Therefore, we have 48 types of TCL to characterize the device colors.

The CTM scheme involves two phases to consecutively receive the collection of the TCL. The first phase called measurement phase is, in sequence, to measure the testing light from each illuminated MCC patch by a Photo Research PR650 spectrophotometer. As a result, the measured color coordinates of CIE 1931 $(x,y,Y)$ for TCL Nos. 1–48 are obtained, as listed in Table 3. The second phase referred to as testing phase is first to acquire the image data from each illuminated MCC patch, and then to evaluate the corresponding camera outputs from these image data.

### 5.3 *Determination of Camera's Colorimetric Model*

From the estimated spectral responsivities of the Sony XC711 camera, the synthesized spectral responsivities are obtained through the spectral matching in Eq. (13) or Eqs. (Ala)–(Alc) from Appendix A. Figure 10 exhibits the comparison between the NTSC-RGB standard and synthesized (or matched) camera's spectral responses. In this figure, the three dash curves, labeled NTSC_R, NTSC_G, and NTSC_B, are the spectral responses of NTSC-RGB standard and the solid curves, marked with CS_R, CS_G, and CS_B, stand for the synthesized spectral responsivities, respectively. From the computation of colorimetric quality, one can see that the degree of the correlation between these two sets of corresponding spectral responses should be consistent with the $q$ factors for RGB channel, since NTSC-RGB standard is a set of color-mixture curves.

In the CTM scheme, the camera outputs can be acquired to constitute the normalized device-color vector $\overline{\mathbf{V}}_C^{(i)} = [\overline{R}_C^{(i)}\ \overline{G}_C^{(i)}\ \overline{B}_C^{(i)}]^{\mathrm{T}} \in \boldsymbol{R}^{3\times 1}$ in response to the $i$th TCL $T_i(\lambda)$, $i=1$ to $N_M$, where $N_M=48$. As described in Sec. 4.2, the reference-white luminance can be determined by solving Eqs. (16)–(20) and Eqs. (B1), (B2), and (B3a)–(B3d) in Appendix B, through numerical calculations. Figure 11 shows the relationship between the reference-white luminance and rms $\Delta E^*_{\mathrm{ab}}$ values, defined in Eq. (19). We obtain the value of the reference-white luminance $Y_0$ equal to 148.22 (cd/m$^2$) at the minimal point of rms $\Delta E^*_{\mathrm{ab}}$. In Fig. 11, we see the effectiveness of determining $Y_0$ since the rms $\Delta E^*_{\mathrm{ab}}=6.1457$ is minimal.

To reduce color errors between the device colors and measured colors that correspond to the TCL $T_i(\lambda)$, $i=1-48$, in the color testing and measurement scheme, we employ the multiple polynomial regression technique, as stated in Sec. 4.3. That is, this technique is used for the color correction. First of all, let's observe color error distributions without color correction. Figure 12 shows the distributions of $\Delta L^*$, $\Delta a^*$, $\Delta b^*$, and $\Delta E^*_{\mathrm{ab}}$ with respect to TCL Nos. 1–48, respectively, and most of $\Delta E^*_{\mathrm{ab}}$ values are larger than 5.

Now, we use the polynomial regression with the degree $j$ ranging from 1 to 3, for color correction. Figures 13(a)–13(c) and 14 exhibit the distributions of $\Delta L^*$, $\Delta a^*$, $\Delta b^*$, and $\Delta E^*_{\mathrm{ab}}$ values, with respect to TCL Nos. 1–48, obtained from the degrees-1, -2, and -3 polynomial regressions for color correction. From Sec. 4, the rms $\Delta E^*_{\mathrm{ab}}$ and the normalized rms $\Delta E^*_{\mathrm{ab}}$ values with color correction are computed in the following:

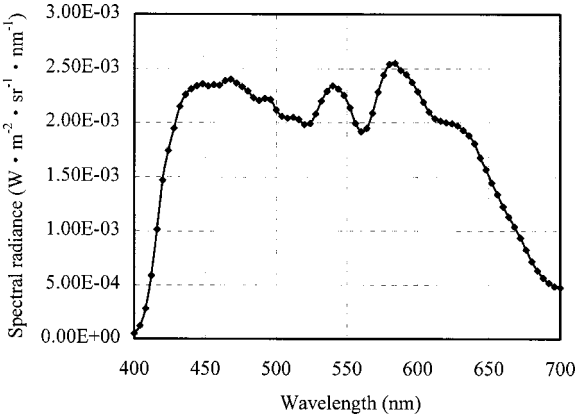


**Fig. 4** Spectral power distribution of the diffused light source.

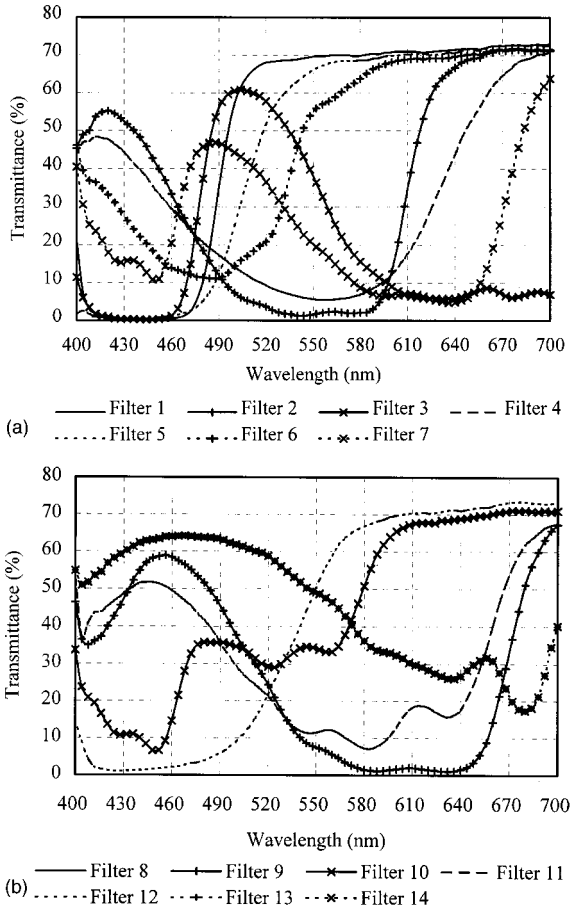


**Fig. 5** (a) A collection of spectral filters (1/2). (b) A collection of spectral filters (2/2).

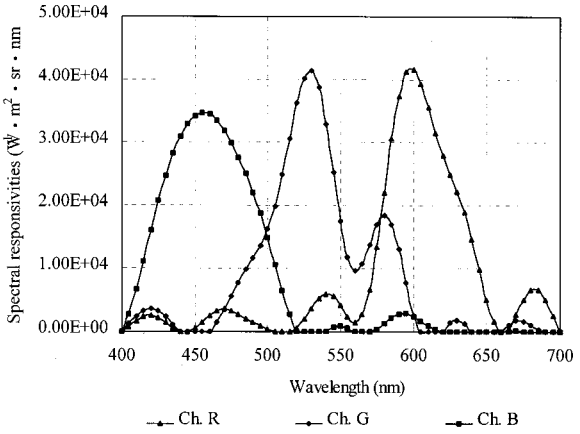


**Fig. 6** Estimated spectral responsivities of a Sony XC711 color camera.

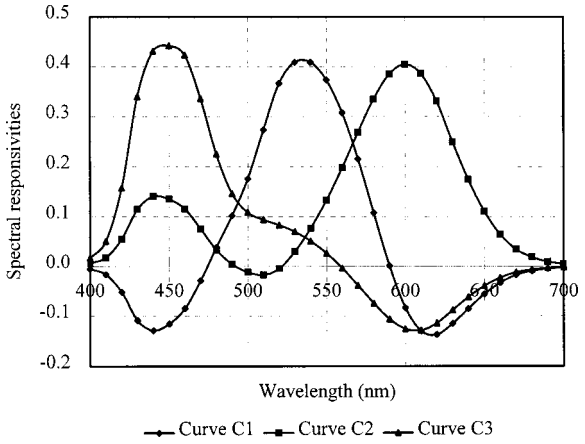


**Fig. 8** A set of orthogonal color-mixture curves suggested by Neugebauer.

$$\text{rms}\ \Delta E^*_{\text{ab}} = \left[ \frac{1}{N_M} \sum_{i=1}^{N_M} (\hat{L}_C^{(i)} - L_M^{(i)})^2 + (\hat{a}_C^{(i)} - a_M^{(i)})^2 + (\hat{b}_C^{(i)} - b_M^{(i)})^2 \right]^{1/2}, \tag{26}$$

and

$$\text{normalized rms}\ \Delta E^*_{\text{ab}} = \sum_{i=1}^{N_M} [(\hat{L}_C^{(i)} - L_M^{(i)})^2 + (\hat{a}_C^{(i)} - a_M^{(i)})^2 + (\hat{b}_C^{(i)} - b_M^{(i)})^2]^{1/2} \Big/ \sum_{i=1}^{N_M} [(L_M^{(i)})^2 + (a_M^{(i)})^2 + (b_M^{(i)})^2]^{1/2}, \tag{27}$$

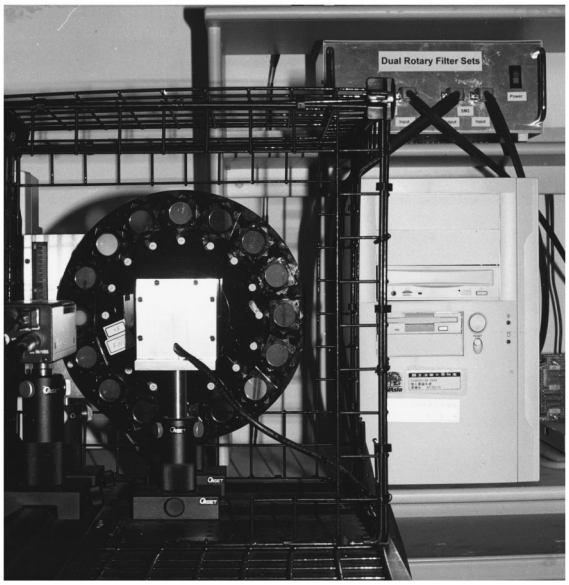


**Fig. 7** Actual installation of the filter-based optical system.

where $(\hat{L}_C^{(i)}, \hat{a}_C^{(i)}, \hat{b}_C^{(i)})$ means the corrected device-color coordinate and $N_M = 48$. Table 4 lists the $\Delta E^*_{\text{ab}}$ values with or without color correction (using polynomial regressions) for the 48 types of TCL. It is found that these color errors dramatically decrease as the degree $j$ increases from 1 to 2. Also, as the degree of the polynomial equals 3, the color differences are smaller than those from the degree 2, but the performance of error reduction is gradually saturated. This implies that the methods of spectral matching and evaluating reference-white luminance, as described in Sec. 4, are essential and effective. That is, only lower-degree polynomial regression is needed to eliminate residual color errors. As shown in Table 4, the normalized rms $\Delta E^*_{\text{ab}}$ values from the polynomial regressions of degrees 1, 2, and 3 are 0.0475, 0.0334, and 0.0267, respectively.

### 5.4 *Performance Verification*

To verify the effectiveness of the colorimetric modeling technique, we employ additional 24 types of colored light and evaluate the color errors corresponding to them. Similar to the CTM scheme, the generation of the colored light is also based on the 0/45 color measurement configuration. The only difference is that we use another daylight-type illuminant with about CCT 5500 K, called an illuminant $D_{55}$, to produce 24 types of colored light, which are different from the TCL Nos. 1–48.

From the camera's colorimetric model, as determined in Sec. 5.3, Table 5 compares the $\Delta E^*_{\text{ab}}$ values with or without color correction (using polynomial regressions) for these types of colored light. For the perceptually uniform color space, CIELAB, it has been shown that a $\Delta E^*_{\text{ab}}$ value of around 2.3 corresponds to a just-noticeable difference[1] (JND). As the degree of polynomial regression equals 3, the rms $\Delta E^*_{\text{ab}} = 2.0475$ is less than a JND, and the corre-

**Table 2** Evaluation results of colorimetric quality factors.

| Channel | Ch. R | Ch. G | Ch. B |
|---|---|---|---|
| Q factor | 0.8930 | 0.8628 | 0.9361 |

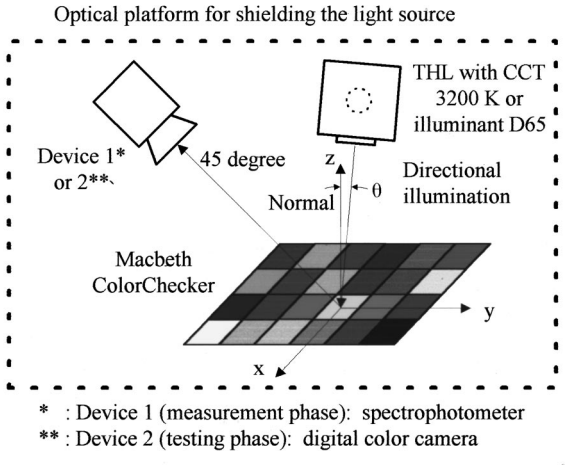


**Fig. 9** Color testing and measurement scheme.

sponding normalized rms $\Delta E^*_{ab}$ is equal to 0.0285. Evidently, our approach incorporated with the polynomial regression of lower degree can effectively diminish the color differences in CIELAB. From the experiments, we can see that if the $q$ factors for color channels are not very poor[5,11] (usually not less than 0.8), the proposed technique can give an accurate colorimetric model for vision systems.

## 6 Conclusions

A computational model of color imaging has been established by the colorimetric modeling technique. First of all, we develop the filter-based optical system for estimating spectral responsivities. According to the camera's spectral responses, the mathematical model of color imaging is determined and then we can evaluate the colorimetric quality factors for the digital camera. In theory, the $q$ factors imply the degree of the correlation between device colors and CIE tristimulus values for human vision. They also indicate the possibility of giving meaningful color representations to an imaging device. That is, if the values of these factors are very low, the performance of color correction is seriously limited due to the poor colorimetric quality.

However, most commercially available imaging devices usually have sufficiently large values of the $q$ factors in specific applications, e.g., in video systems or television industry. Therefore, knowing the colorimetric quality is beneficial to this work. In our approach, the colorimetric modeling process primarily involves three methods for color characterization. They are the spectral matching, reference-white luminance determination, and polynomial regression methods. In particular, from the selection of polynomial degree, we see the effectiveness of the first two methods. Specifically, we only need to use lower-degree polynomial regression for color correction. These three methods are expressed by individually specified functions. Then, these functions are incorporated into the mathematical model, with the estimated spectral responses, for camera imaging and consequently the colorimetric model for vision systems is established. Therefore, we can see that the proposed technique achieves a satisfactory accuracy for the colorimetric model.

## Appendix A

Let $\hat{\mathbf{m}}_i = [\hat{\alpha}_{i1}\ \hat{\alpha}_{i2}\ \hat{\alpha}_{i3}]^T \in \boldsymbol{R}^{3\times 1}$, for $i = 1, 2, 3$. From Eq. (13), we have

$$\hat{\alpha}_{11}R_S(\lambda) + \hat{\alpha}_{12}G_S(\lambda) + \hat{\alpha}_{13}B_S(\lambda) = R_C(\lambda), \tag{A1a}$$

$$\hat{\alpha}_{21}R_S(\lambda) + \hat{\alpha}_{22}G_S(\lambda) + \hat{\alpha}_{23}B_S(\lambda) = G_C(\lambda), \tag{A1b}$$

and

**Table 3** CIE 1931 $(x, y, Y)$ coordinates of the 48 types of testing color light.

| TCL No. | $x$ | $y$ | $Y$ |
|---|---|---|---|
| 1 | 0.506 | 0.396 | 11.68 |
| 2 | 0.492 | 0.397 | 41.63 |
| 3 | 0.357 | 0.362 | 19.40 |
| 4 | 0.427 | 0.465 | 15.00 |
| 5 | 0.390 | 0.349 | 25.94 |
| 6 | 0.352 | 0.440 | 43.40 |
| 7 | 0.566 | 0.402 | 39.15 |
| 8 | 0.310 | 0.290 | 12.25 |
| 9 | 0.565 | 0.350 | 27.42 |
| 10 | 0.428 | 0.318 | 7.69 |
| 11 | 0.450 | 0.490 | 50.34 |
| 12 | 0.535 | 0.432 | 55.62 |
| 13 | 0.260 | 0.228 | 5.82 |
| 14 | 0.380 | 0.517 | 24.69 |
| 15 | 0.625 | 0.330 | 17.85 |
| 16 | 0.509 | 0.456 | 73.10 |
| 17 | 0.521 | 0.316 | 25.52 |
| 18 | 0.275 | 0.371 | 17.89 |
| 19 | 0.427 | 0.401 | 101.12 |
| 20 | 0.425 | 0.402 | 65.24 |
| 21 | 0.425 | 0.401 | 39.07 |
| 22 | 0.422 | 0.402 | 21.50 |
| 23 | 0.421 | 0.402 | 9.57 |
| 24 | 0.424 | 0.400 | 3.27 |
| 25 | 0.389 | 0.356 | 10.64 |
| 26 | 0.371 | 0.355 | 39.83 |
| 27 | 0.244 | 0.257 | 21.64 |
| 28 | 0.328 | 0.424 | 15.73 |
| 29 | 0.260 | 0.248 | 27.43 |
| 30 | 0.259 | 0.352 | 49.34 |
| 31 | 0.491 | 0.410 | 30.54 |
| 32 | 0.208 | 0.178 | 13.25 |
| 33 | 0.436 | 0.312 | 21.49 |
| 34 | 0.270 | 0.212 | 6.95 |
| 35 | 0.374 | 0.490 | 49.91 |
| 36 | 0.463 | 0.444 | 51.20 |
| 37 | 0.187 | 0.139 | 7.25 |
| 38 | 0.307 | 0.481 | 26.87 |
| 39 | 0.513 | 0.318 | 12.05 |
| 40 | 0.438 | 0.477 | 66.95 |
| 41 | 0.346 | 0.235 | 20.74 |
| 42 | 0.196 | 0.259 | 20.91 |
| 43 | 0.307 | 0.325 | 101.52 |
| 44 | 0.306 | 0.325 | 67.02 |
| 45 | 0.305 | 0.322 | 40.28 |
| 46 | 0.303 | 0.323 | 22.18 |
| 47 | 0.303 | 0.322 | 9.66 |
| 48 | 0.302 | 0.320 | 3.45 |

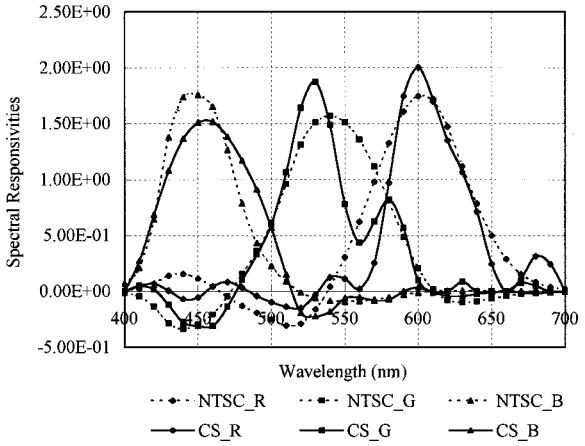


**Fig. 10** Comparison between the NTSC-RGB standard and synthesized camera's spectral responses from the spectral matching.

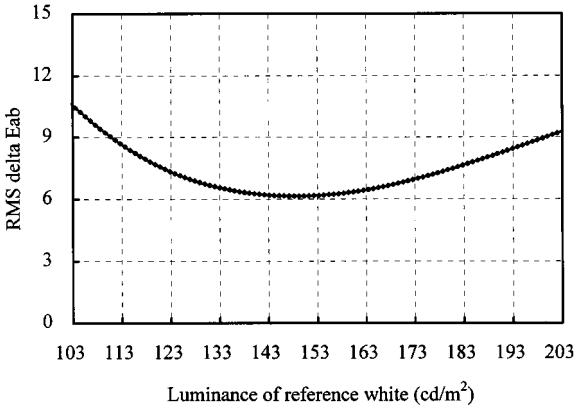


**Fig. 11** The relationship between the reference-white luminance and rms $\Delta E^*_{ab}$ values.

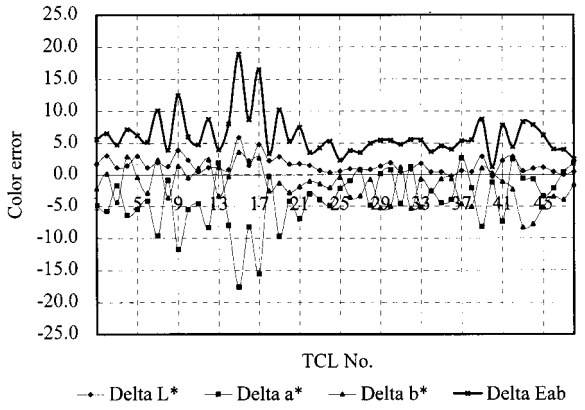


**Fig. 12** Distributions of $\Delta L^*$, $\Delta a^*$, $\Delta b^*$, and $\Delta E^*_{ab}$ values without color correction using polynomial regressions.

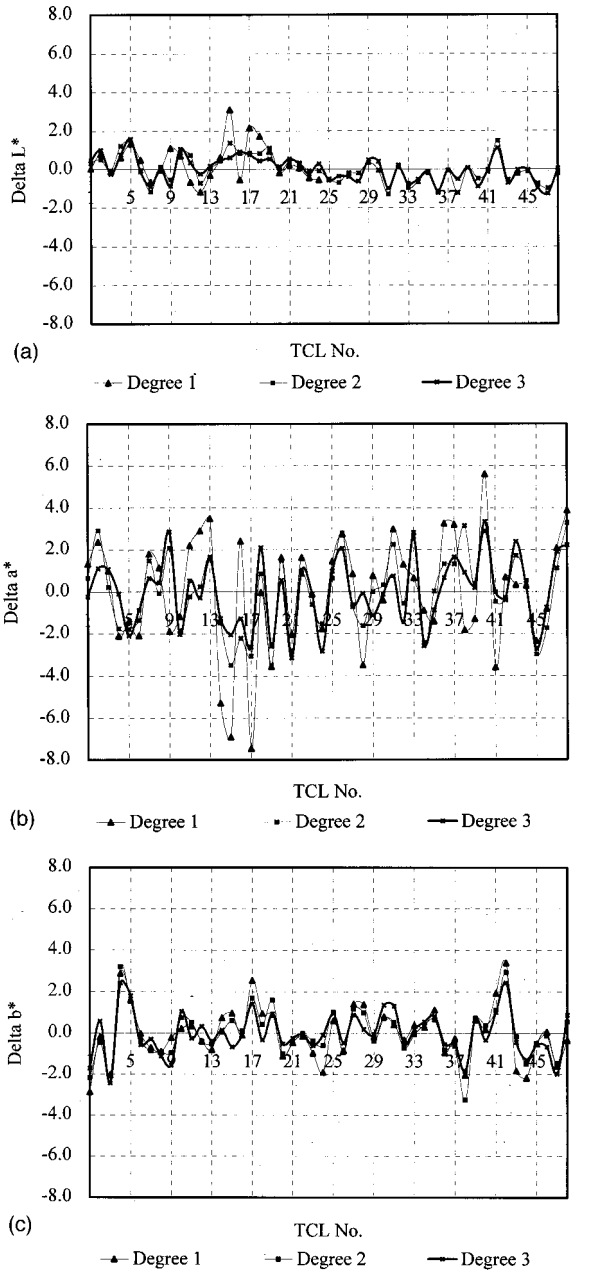


**Fig. 13** (a) Distributions of $\Delta L^*$ values corrected with polynomial regressions. (b) Distributions of $\Delta a^*$ values corrected with polynomial regressions. (c) Distributions of $\Delta b^*$ values corrected with polynomial regressions.

$$\hat{\alpha}_{31}R_S(\lambda)+\hat{\alpha}_{32}G_S(\lambda)+\hat{\alpha}_{33}B_S(\lambda)=B_C(\lambda). \qquad \text{(A1c)}$$

It is reasonably assumed that the noise effect may be negligible if the average of repeated observations from camera outputs is taken for the same incident light and if the mean value of camera noise is zero. For the $i$th testing incident light $T_i(\lambda)$, by taking spectral integration on both sides of Eqs. (A1a)–(A1c) over the visible range $[\lambda_1,\lambda_2]$, the camera output yields

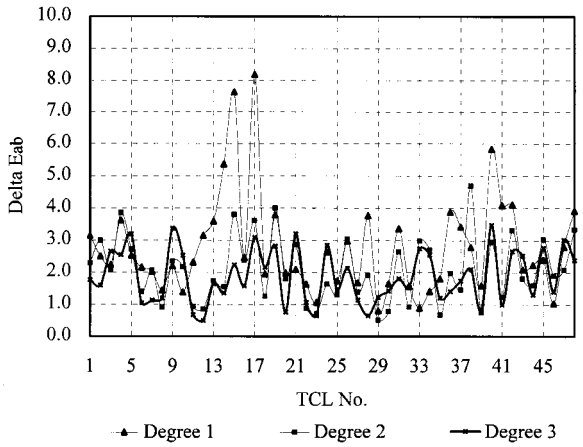


**Fig. 14** Distributions of $\Delta E^*_{ab}$ values corrected with polynomial regressions.

$$[R_C^{(i)}\ G_C^{(i)}\ B_C^{(i)}]^{\mathrm{T}}=\hat{\mathbf{M}}_S^{\mathrm{T}}[(R_S^{(i)}-\beta_R)\ (G_S^{(i)}-\beta_G)(B_S^{(i)}-\beta_B)]^{\mathrm{T}},\quad i=1,\ 2,...,N_M, \tag{A2}$$

where $R_C^{(i)}=\int_{\lambda_1}^{\lambda_2}T_i(\lambda)R_C(\lambda)d\lambda$, $G_C^{(i)}=\int_{\lambda_1}^{\lambda_2}T_i(\lambda)G_C(\lambda)\times d\lambda$, and $B_C^{(i)}=\int_{\lambda_1}^{\lambda_2}T_i(\lambda)B_C(\lambda)d\lambda$, and $R_S^{(i)}-\beta_R=\int_{\lambda_1}^{\lambda_2}T_i(\lambda)R_S(\lambda)d\lambda$, $G_S^{(i)}-\beta_G=\int_{\lambda_1}^{\lambda_2}T_i(\lambda)G_S(\lambda)d\lambda$, and $B_S^{(i)}-\beta_B=\int_{\lambda_1}^{\lambda_2}T_i(\lambda)B_S(\lambda)d\lambda$ can be obtained from Eq. (3) without the effect of camera noise.

To normalize the computed camera output from Eq. (14), after the spectral matching, it is found that

$$[\overline{R}_C^{(i)}\ \overline{G}_C^{(i)}\ \overline{B}_C^{(i)}]^{\mathrm{T}}=\hat{\hat{\mathbf{M}}}_S^{\mathrm{T}}[\overline{R}_S^{(i)}\ \overline{G}_S^{(i)}\ \overline{B}_S^{(i)}]^{\mathrm{T}},\quad i=1\ \text{ to }\ N_M, \tag{A3}$$

where $\hat{\hat{\mathbf{M}}}_S=[\hat{\hat{\mathbf{m}}}_1\ \hat{\hat{\mathbf{m}}}_2\ \hat{\hat{\mathbf{m}}}_3]\in\boldsymbol{R}^{3\times3}$, $\hat{\hat{\mathbf{m}}}_k=[\hat{\alpha}_{k1}\ \hat{\alpha}_{k2}\ \hat{\alpha}_{k3}]^{\mathrm{T}}\times(\Sigma_{j=1}^{3}\hat{\alpha}_{kj})^{-1}$, $k=1$, 2, 3, and $\overline{R}_S^{(i)}$, $\overline{G}_S^{(i)}$, and $\overline{B}_S^{(i)}$ are the normalized values of the trimmed camera outputs; e.g.,

$$\overline{R}_S^{(i)}=(R_S^{(i)}-\beta_R)/(R_{\max}-\beta_R), \tag{A4}$$

and $R_{\max}$ represents the full scale of data representation for channel $R$. The full scales of $n$-bit unsigned binary numbers for RGB channels are usually equal to $2^n-1$. From Eq. (A3), it is obvious that $\overline{R}_C^{(i)}=\overline{G}_C^{(i)}=\overline{B}_C^{(i)}=1$, if $\overline{R}_S^{(i)}=\overline{G}_S^{(i)}=\overline{B}_S^{(i)}=1$. The manipulation from Eq. (A4) is referred to as the trimming and normalization of device colors.

**Table 4** Evaluation of $\Delta E^*_{ab}$ values with or without color correction (using polynomial regressions) for the 48 types of TCL.

| Types of polynomial regression | Normalized rms $\Delta E^*_{ab}$ | rms $\Delta E^*_{ab}$ | Max. $\Delta E^*_{ab}$ |
|---|---|---|---|
| No polynomial regression | 0.1022 | 6.1457 | 18.8884 |
| Degree 1 | 0.0475 | 2.8586 | 8.1821 |
| Degree 2 | 0.0334 | 2.0075 | 4.6846 |
| Degree 3 | 0.0267 | 1.7282 | 3.4739 |

**Table 5** Comparison of $\Delta E^*_{ab}$ values with or without color correction (using polynomial regressions) for additional 24 types of colored light.

| Types of polynomial regression | Normalized rms $\Delta E^*_{ab}$ | rms $\Delta E^*_{ab}$ | Max. $\Delta E^*_{ab}$ |
|---|---|---|---|
| No polynomial regression | 0.0872 | 5.3511 | 10.7934 |
| Degree 1 | 0.0380 | 2.7328 | 6.0596 |
| Degree 2 | 0.0314 | 2.2647 | 5.9787 |
| Degree 3 | 0.0285 | 2.0475 | 4.8437 |

## Appendix B

For the $i$th normalized vector $[\overline{R}_C^{(i)}\ \overline{G}_C^{(i)}\ \overline{B}_C^{(i)}]^{\mathrm{T}}\in\boldsymbol{R}^{3\times1}$, the transformation from NTSC-RGB (with illuminant $D_{65}$) to CIE$XYZ$ can be expressed as[17,19]

$$\overline{\mathbf{V}}_X^{(i)}=[\overline{X}_C^{(i)}\ \overline{Y}_C^{(i)}\ \overline{Z}_C^{(i)}]^{\mathrm{T}}=\overline{\mathbf{M}}_X\overline{\mathbf{V}}_C^{(i)}=\mathbf{M}_X[\overline{R}_C^{(i)}\ \overline{G}_C^{(i)}\ \overline{B}_C^{(i)}]^{\mathrm{T}}\in\boldsymbol{R}^{3\times1},\quad i=1\ \text{ to }\ N_M, \tag{B1}$$

where

$$\overline{\mathbf{M}}_X=\begin{bmatrix}0.5881 & 0.1791 & 0.1832\\ 0.2897 & 0.6056 & 0.1047\\ 0 & 0.682 & 1.0209\end{bmatrix}.$$

It is noted that as $\overline{R}_C^{(i)}=\overline{G}_C^{(i)}=\overline{B}_C^{(i)}=1$, Eq. (B1) gives unit luminance, i.e., $\overline{Y}_C^{(i)}=1$. Obviously, a function $\Phi_X(\cdot)$ can be designated for this transformation, i.e.,

$$\overline{\mathbf{V}}_X^{(i)}=\Phi_X(\overline{\mathbf{V}}_C^{(i)}). \tag{B2}$$

The transformation from the CIE$XYZ$ coordinate $(X,Y,Z)$ to the CIELAB coordinate $(L^*,a^*,b^*)$ can be formulated as[17,19]

$$L^*=116f(Y/Y_0)-16, \tag{B3a}$$

$$a^*=500[f(X/X_0)-f(Y/Y_0)], \tag{B3b}$$

and

$$b^*=200[f(Y/Y_0)-f(Z/Z_0)], \tag{B3c}$$

where

$$f(\gamma)=\begin{cases}\sqrt[3]{\gamma}, & \gamma>0.008\,856,\\ 7.787\gamma+\frac{16}{116}, & \gamma\leqslant0.008\,856,\end{cases} \tag{B3d}$$

$X_0$, $Y_0$, and $Z_0$ are the tristimulus values of illuminant $D_{65}$. Specifically, the value of $Y_0$ is the luminance of this reference white. Similar to Eq. (B2), this transformation can be expressed as a function $\Phi_L(\cdot)$. That is, for the vector $\overline{\mathbf{V}}_X^{(i)}=[\overline{X}_C^{(i)}\ \overline{Y}_C^{(i)}\ \overline{Z}_C^{(i)}]^T \in \boldsymbol{R}^{3\times 1}$, we have

$$\mathbf{V}_L^{(i)}=\Phi_L(\overline{\mathbf{V}}_X^{(i)}),\quad i=1\ \text{ to }\ N_M, \tag{B4}$$

where $\mathbf{V}_L^{(i)}=[L_C^{(i)}\ a_C^{(i)}\ b_C^{(i)}]^T \in \boldsymbol{R}^{3\times 1}$.

## Acknowledgments

This work was supported by National Science Council, Taiwan, Republic of China (R.O.C), under Grant No. NSC 87-2213-E-007-060. The first author would like to deeply express his appreciation to both the Optical-Electronics and Systems Laboratory and the Center for Measurement Standards in the Industrial Technology Research Institute (ITRI) for invaluable working experience with them.

## References

1. G. Sharma H. J. Trussell, ''Digital color imaging,'' *IEEE Trans. Image Process.* **6**(7), 901–932 (1997).
2. M. Jackowski *et al.*, ''Correcting the geometry and color of digital images,'' *IEEE Trans. Pattern Anal. Mach. Intell.* **19**(10), 267–276 (1997).
3. M. J. Vrhel and H. J. Trussell, ''Color correction using principle components,'' *Color Res. Appl.* **17**(5), 328–338 (1992).
4. C. L. Novak, S. A. Shafer, and R. G. Willson, ''Obtaining accurate color images for machine vision research,'' in *Physics-Based Vision: Principle and Practice-Color*, G. E. Healey, S. A. Shafer, L. B. Wolff, Eds., pp. 13–27, Jones and Bartlett, Boston, MA (1992).
5. P. L. Vora and H. J. Trussell, ''Measure of goodness of a set of color-scanning filters,'' *J. Opt. Soc. Am. A* **10**(7), 1499–1508 (1993).
6. M. Wolski, C. A. Bouman, J. P. Allebach, E. Walowit, ''Optimization of sensor response functions for colorimetry of reflective and emissive objects,'' *IEEE Trans. Image Process.* **5**(3), 507–517 (1996).
7. P. G. Herzog *et al.*, ''Colorimetric characterization of novel multiple-channel sensors for imaging and metrology,'' *J. Electron. Imaging* **8**(4), 342–353 (1999).
8. K. Engelhardt and P. Seitz, ''Optimum color filters for CCD digital cameras,'' *Appl. Opt.* **32**(16), 3015–3023 (1993).
9. H. R. Kang, ''Color scanner calibration,'' *J. Imaging Sci. Technol.* **36**(2), 162–170 (1992).
10. R. J. Green and S. J. Ismail, ''Color error reduction in video systems,'' *IEEE Trans. Broadcasting*, **36**(1), 99–107 (1990).
11. S. Suzuki, M. Tsuda, and M. Mori, ''A filter-alternating color scanner,'' *Fujitsu Sci. Tech. J.* **25**(4), 279–286 (1990).
12. Y. C. Chang and J. F. Reid, ''RGB calibration for color image analysis in machine vision,'' *IEEE Trans. Image Process.* **5**(10), 1414–1422 (1996).
13. G. E. Healey and R. Kondepudy, ''Radiometric CCD camera calibration and noise estimation,'' *IEEE Trans. Pattern Anal. Mach. Intell.* **16**(3), 267–276 (1994).
14. M. J. Vrhel and H. J. Trussell, ''Color device calibration: a mathematical formulation,'' *IEEE Trans. Image Process.* **8**(12), 1796–1806 (1999).
15. R. Lenz, P. Meer, M. Hauta-Kasari, ''Spectral-based illumination estimation and color correction,'' *Color Res. Appl.* **24**(2), 98–111 (1999).
16. G. W. Chang and Y. C. Chen, ''Spectral estimation of color CCD cameras,'' in Input/Output and Imaging Techniques, *Proc. SPIE* **3422**, 81–91 (1998).
17. J. A. C. Yule, *Principles of Color Reproduction*, Wiley, New York (1967) (reprinted in 1989).
18. W. N. Sproson, *Color Science in Television and Display Systems*, Adam Hilger Ltd., Bristol (1983).
19. G. Wyszecki and W. S. Stiles, *Color Science—Concepts and Methods, Quantitative Data and Formulae*, Wiley, New York (1982).
20. G. H. Golub and C. F. Van Loan, *Matrix Computations*, 2nd ed., John Hopkins University Press, Baltimore (1989).
21. C. L. Lawson and R. J. Hanson, *Solving Least Squares Problems*, Prentice-Hall, Englewood Cliffs, NJ (1974).
22. A. V. Oppenheim and R. W. Schafer, *Discrete-Time Signal Processing*, Prentice Hall, Englewood Cliffs, NJ (1989).

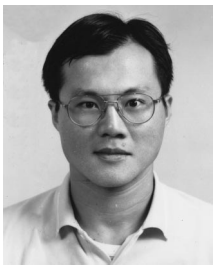

**Gao-Wei Chang** graduated from National Taipei Institute of Technology, Taipei, R.O.C., in 1985 and received an MS degree in the Department of Electrical Engineering of National Tsing Hua University (NTHU), Hsinchu, Taiwan, in 1991. He is currently a Ph.D. student in NTHU. From 1991 to 1995, he was an electronics engineer in charge of color image processing in the Opto-Electronics and Systems Laboratory of Industrial Technology Research Institute (ITRI), Taiwan. From 1995 to 1998, he was an opto-electronics engineer in the Optical Metrology Laboratory of the Center for Measurement Standards, ITRI, Taiwan. His research interests include color image processing, electro-optical systems, automatic testing and measurement systems, and artificial intelligence.

**Yung-Chang Chen** received BS and MS degrees in electrical engineering from the National Taiwan University, Taipei, in 1968 and 1970, respectively, and Dr.Ing. degree from Berlin Technical University, Berlin, Germany, in 1978. Since 1978, he has been with the Department of Electrical Engineering, National Tsing Hua University, Taiwan, R.O.C., where he is currently a professor. His research interests are image processing, pattern recognition, signal processing, medical image processing, and video coding.